IEEE Access
Multidisciplinary | Rapid Review | Open Access Journal

Received October 24, 2019, accepted November 14, 2019, date of publication November 27, 2019,
date of current version December 12, 2019.

*Digital Object Identifier 10.1109/ACCESS.2019.2956164*

# Deformable Terrain Model for the Real-Time Multibody Simulation of a Tractor With a Hydraulically Driven Front-Loader

**SURAJ JAISWAL[1], PASI KORKEALAAKSO[2], RAFAEL ÅMAN[3], JUSSI SOPANEN[1], (Member, IEEE), AND AKI MIKKOLA[1]**

[1]Department of Mechanical Engineering, Lappeenranta University of Technology, 53850 Lappeenranta, Finland
[2]Mevea Ltd., 53850 Lappeenranta, Finland
[3]Valtra Inc., 44200 Suolahti, Finland

Corresponding author: Suraj Jaiswal (suraj.jaiswal@lut.fi)

This work was supported in part by the Business Finland [project: Digital Product Processes through Physics Based Real-Time Simulation—DigiPro], and in part by the Academy of Finland under Grant #316106.

**ABSTRACT** A real-time multibody model of an off-road vehicle can be used to analyze the dynamics of tasks, such as loading and/or transferring material from deformable ground. This analysis requires an accurate description of the mechanics, hydraulic actuators, and the terrain. The objective of this paper is to introduce a novel, real-time capable, deformable terrain/soil model that can interact with the mechanics of a multibody system model and the dynamics of a hydraulics model. To this end, a tractor is modeled by using a semi-recursive multibody formulation based on velocity transformation. The hydraulic actuation of the tractor's front-loader is modeled by using the lumped fluid theory. The tractor loads and transfers sand material from a deformable sand field (the ground), which is modeled by combining mesh-based and particle-based soil representation approaches for the real-time simulation of soil deformation. The work cycle of the tractor model follows a 3D maneuver that is used to load and transfer sand material. During the digging and dumping operations, the static sand field is converted into sand particles and vice versa respectively. For the presented work cycle, the real-time capability of the system is analyzed and determined. Furthermore, the dynamic actuator forces in the hydraulic cylinders are compared with the static actuator forces. The introduced real-time capable tractor simulation model can be utilized in product development and other product processes.

**INDEX TERMS** Deformable soil/terrain model, hydraulic actuators, multibody system dynamics, real-time simulation, semi-recursive formulation, vehicle dynamics.

## I. INTRODUCTION

A real-time multibody system dynamics approach can be used to analyze the dynamic behavior of an off-road vehicle, such as a tractor [1]. A tractor with a hydraulically actuated front-loader can interact with its environment in two ways. It can either collide with the scene's objects and terrain, or it can load and/or transfer materials such as soil (the terrain) onto another type of machinery. To load and/or transfer material is a common task for a tractor, and for such an operation, the hydraulic actuators and the wheel/track/bucket and terrain interaction plays a major role in the tractor's dynamic performance. To achieve a real-time capable, realistic model with which to analyze the dynamics, an accurate description of the mechanical model, hydraulics model, and terrain model is needed.

In the literature, there are a large number of papers showing that multibody system dynamics can be coupled with a hydraulic system in the application of mobile machines. For example, Panetta *et al.* [2] presented a virtual tool (software) that coupled a multibody model of a tractor and a detailed hydraulic model of the suspension system in order to tune the hydro-pneumatic semi-active suspension system of the tractor. The hydraulic suspension system accounted for the dynamics of the electro-hydraulic valves, accumulator, and hydraulic actuator of the tractor. The model

The associate editor coordinating the review of this manuscript and approving it for publication was Fabrizio Messina.

was validated by comparing it against experimental data from leveling and dynamic bump tests conducted on the tractor. Baharudin *et al.* [3] demonstrated a combination of multibody system dynamics and hydraulics modeling for the real-time simulation of a hydraulically driven tree harvester. They utilized a semi-recursive formulation [4] for the dynamic modeling of the mechanical system and the lumped fluid theory [5] for modeling the hydraulic circuits. Contacts in this approach were described using the penalty approach. Jaiswal *et al.* [6] modeled a hydraulically actuated excavator to demonstrate a real-time capable, multibody simulation-based gamification procedure. They utilized the same semi-recursive formulation [4] and lumped fluid theory [5] in their study. Rahikainen *et al.* [7] introduced a monolithic formulation for a combined simulation of multibody and hydraulic dynamics by utilizing a semi-recursive formulation [8] and the lumped fluid method [5]. As a test case, they studied a four-bar linkage and a double-acting cylinder, a mechanism that is commonly used in hydraulic actuated machinery. Cook *et al.* [9] presented a generalized, multibody dynamics model of a quadtrac, which was equipped with a hydraulically powered towing winch for optimal mobility control and terrain identification. They utilized the Newton–Euler method in the system modeling. The model was used to recognize the limitation of the winch as an actuator and the amount of load it applied on the engine. Furthermore, Zou *et al.* [10] proposed a convex, polytope-based method in order to evaluate the theoretical digging performance (forces and moments) of a hydraulic excavator in the bucket force space. Newton–Euler equations were used to establish the dynamic relationships between the digging capability of the bucket and the driving capability of the hydraulic cylinder. Of the studies [2], [3], [6], [7], [9], the hydraulics modeling utilized by Baharudin *et al.* [3], Jaiswal *et al.* [6], and Rahikainen *et al.* [7] is applicable for real-time applications.

A number of studies in the literature have introduced ways to couple multibody system dynamics to terrain/soil modeling for a complex mobile machine. For example, Nicolini *et al.* [11] studied a multibody model of a small-sized tracked farming vehicle on two different types of soil: sand and compact agricultural terrain. The soil field was modeled as a rigid body and its motion was kinematically related to the vehicle so that the soil model moved under the vehicle near the tracks. The terramechanics equations of Bekker [12] and Janosi and Hanamoto [13] were utilized to describe the normal and tangential forces between the track and soil. Ma and Perkins [14] utilized the same terramechanics equations in their study. They proposed a track–wheel–terrain interaction model by using a nonlinear, finite element representation of the track segment and an adapting meshing scheme. As a test case, they studied the dynamics of a full vehicle model of an M1A1 tank on rough terrain, such as LETE sand. Sandu *et al.* [15], [16] investigated the modeling of a complex nonlinear multibody system in the presence of parametric and external uncertainties, such as vehicle–soil interaction. They utilized generalized polynomial chaos theory for the study. The methodology was illustrated on a quarter car model [16]. They demonstrated a stochastic terrain model by utilizing a truncated Karhunen–Loeve expansion [16]. However, the soil models in these studies [11]–[14] were unsuitable for real-time applications. However, Holz *et al.* [17] proposed a hybrid method for the real-time simulation of soil deformation, but not in the framework of multibody system dynamics. A high degree of soil dynamics (soil compaction and erosion) was accounted for in their study.

Dopico *et al.* [18] made an attempt to couple multibody system dynamics with terrain/soil modeling for a medium-sized wheeled excavator. In addition, they modeled the hydraulic cylinders as kinematic constraints and ignored the dynamics of the hydraulic actuators. The used multibody formulation was an index-3 augmented Lagrangian with projections of velocities and acceleration onto the constraint manifolds [19]. The contact forces were modeled as a normal force model (the Hunt–Crossley model [20]) and tangential force model [21]. The dynamic model (with 17 degrees of freedom) was real-time capable and was able to perform terrain excavation. The soft soil was modeled as a terrain mesh. However, they introduced only a simplified bucket-filling model for real-time purposes and they ignored the material flow aspect, that is, the soil model was not real-time capable.

In the literature, a number of studies have been carried out regarding soft terrain modeling for real-time applications. He *et al.* [22] aimed to standardize the experimental procedures that are used for the measurement of soil parameters and for the parameterization of terramechanics models. A comprehensive literature review was conducted to study the soil parameters, modeling procedures, experimental methods, and equipment that are used by the International Society of Terrain–Vehicle Systems community. Their study summarized the modeling techniques that are suitable for the real-time applications of terramechanics in simulation. Madsen *et al.* [23] developed a three-dimensional, physics-based, tire-terrain interaction model that can be used for off-road vehicle simulations in real time. The tire model was based on a lumped mass approach that utilized a radial spring-damper-mass distribution. The soil model utilized Boussinesq and Cerruti soil mechanics equations to compute the deformation of a volume of soil and the pressure distribution in terms of the vertical and lateral forces applied by the tire at the soil surface. In their study, numerical experiments were performed on a single soil volume node under the normal force applied by the simplified tire model on the surface of the soil. Jain *et al.* [24] focused on the description of the Rover Analysis, Modeling, and Simulation (ROAMS) system that is used to develop rover vehicles for planetary surface exploration. The ROAMS system provided real-time simulation of a planetary rover over deformable terrain. The terrain model applied the fundamental soil mechanics models, such as Mohr–Coulomb failure criterion equations [25]. Studies have also been carried out in the area of space robotics.

For example, Azimi *et al.* [26] proposed a novel approach, based on the elastoplasticity theory, to model the rigid-wheel and soft-soil interaction for rover simulation and analysis. They utilized the velocity field for soil particles (near the contact region) and the modified Drucker–Prager model to determine the normal and shear stress field in the contact area. Their study showed good agreement with the experimental data available from the literature and with the Bekker [12] and Wong–Reece [27] models. The model was compatible with multibody dynamics environments and its efficiency makes it suitable for the real-time simulation of rovers on soft soil. However, they focused on robotic systems that moved slowly, that is, with a rover speed of a few centimeters per second. Even though [22]–[24], [26] focused mainly on the wheel–terrain interaction models, the soft soil/terrain models developed by [23], [24], [26] are applicable for real-time applications, but are limited to tire–soil contacts only.

From the literature review, it can be concluded that there are a number of studies concerning terrain/soil models and hydraulics models within the multibody system dynamics framework that are appropriate for real-time applications. However, a real-time capable terrain/soil model that couples a detailed multibody dynamic system and a hydraulic system for complex mobile machines has been overlooked. Accordingly, the objective of this paper is to introduce a novel, real-time capable, deformable terrain/soil model that can interact with the mechanics of a multibody system model and the dynamics of a hydraulics model. The terrain/soil model can interact with any object, such as a bucket, along with the tires. To this end, a tractor will be described by using a semi-recursive multibody formulation based on velocity transformation [4]. The hydraulic actuation of the tractor's front-loader will be described by using the lumped fluid theory. The tractor will load and transfer sand material from a deformable sand field (ground) that will be described by combining mesh-based and particle-based soil representation methods for the real-time simulation of soil deformation. In addition, the contact model will be described by using the object-oriented bounding box method and penalty method, and the tire model will be described by using the lumped LuGre model. As a numerical example, the tractor's dynamic behavior on the deformable ground will be analyzed. Such a real-time capable simulation model can be utilized for product development and other product processes.

## II. MULTIBODY FORMULATION

The equations of motion for a constrained mechanical system can be illustrated by using a multibody system dynamics approach. In multibody system dynamics, a number of formulations can be employed to construct the equations of motion, such as the augmented Lagrangian formulation [28], penalty formulation [29], recursive formulation [30], and semi-recursive formulation [4], [31]. In this study, a semi-recursive formulation based on a velocity transformation [4] is used because it provides a computationally efficient approach for vehicle applications, making it suitable for real-time applications. A combination of mesh-based and particle-based methods are used to model a deformable terrain. Lumped fluid theory [5], in turn, is used to model the hydraulic actuators. Furthermore, the object-oriented bounding box method [32] and penalty method [33] are used to model collision detection and response, and the lumped LuGre model [34], [35] is used to model the tire–ground contact.

### A. SEMI-RECURSIVE MULTIBODY FORMULATION

In this study, the equations of motion are initially derived in terms of translational and rotational generalized coordinates, which are later projected onto the joint coordinate space using a velocity transformation matrix [4]. Consider two adjacent rigid bodies, $B_{j-1}$ and $B_j$ in an open-loop system of $N_b$ bodies with any number of branches (tree-structure mechanisms), connected by a joint, as shown in Fig. 1. The locations of the joint on bodies $B_{j-1}$ and $B_j$ are denoted by points $Q$ and $P$ respectively. The joint relative displacement vector between points $Q$ and $P$ is denoted by $\mathbf{d}_{j-1,j}$.

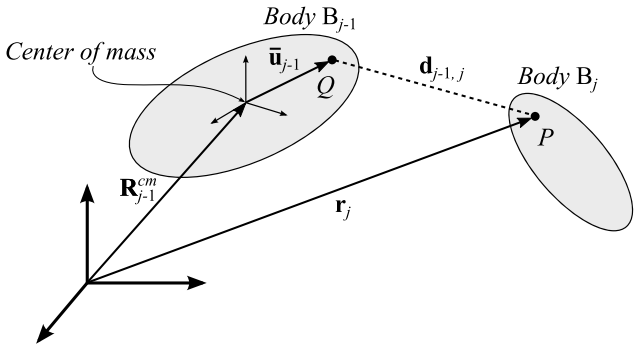


**FIGURE 1. Illustration of two adjacent rigid bodies connected by a joint in an open-loop system.**

The position $\mathbf{r}_j$ of point $P$ in the global reference frame can be expressed as

$$\mathbf{r}_j = \mathbf{R}^{cm}_{j-1} + \mathbf{A}_{j-1}\bar{\mathbf{u}}_{j-1} + \mathbf{d}_{j-1,j} \tag{1}$$

where $\mathbf{R}^{cm}_{j-1}$ is the position of the body reference frame of body $B_{j-1}$ with respect to the global reference frame, $\mathbf{A}_{j-1}$ is the rotation matrix of body $B_{j-1}$, and $\bar{\mathbf{u}}_{j-1}$ is the location of point $Q$ in the body reference frame of body $B_{j-1}$. Note that the body reference frame is located at the center of mass of the body. The rotation matrix of body $B_j$ can be expressed as

$$\mathbf{A}_j = \mathbf{A}_{j-1}\mathbf{A}_{j-1,j} \tag{2}$$

where $\mathbf{A}_{j-1,j}$ is the relative rotation matrix between the two bodies. In this study, body rotation is described by using the Euler parameters. Similar to (1), the velocities expression can be written as

$$\dot{\mathbf{r}}_j = \dot{\mathbf{R}}^{cm}_{j-1} + \tilde{\boldsymbol{\omega}}_{j-1}\mathbf{u}_{j-1} + \dot{\mathbf{d}}_{j-1,j} \tag{3}$$

$$\boldsymbol{\omega}_j = \boldsymbol{\omega}_{j-1} + \boldsymbol{\omega}_{j-1,j} \tag{4}$$

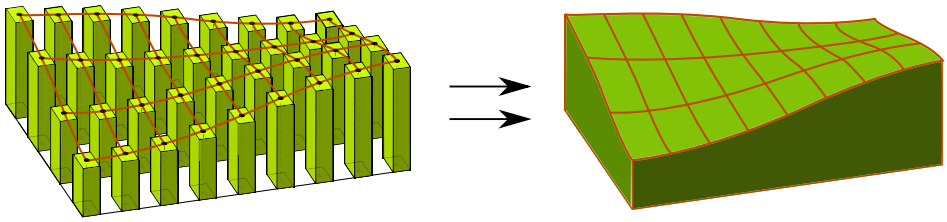


**FIGURE 2.** The soil model in a static state is defined as cells in a grid (heightfield). The center located on top of each soil column is referred to as the *heightfield vertex*.

where $\dot{\mathbf{r}}_j$, $\dot{\mathbf{R}}^{cm}_{j-1}$, and $\dot{\mathbf{d}}_{j-1,j}$ are, respectively, the time derivatives of $\mathbf{r}_j$, $\mathbf{R}^{cm}_{j-1}$, and $\mathbf{d}_{j-1,j}$; $\boldsymbol{\omega}_{j-1}$ and $\boldsymbol{\omega}_j$ are, respectively, the angular velocities of bodies $\mathrm{B}_{j-1}$ and $\mathrm{B}_j$; $\mathbf{u}_{j-1} = \mathbf{A}_{j-1}\bar{\mathbf{u}}_{j-1}$. In (3), $\widetilde{\boldsymbol{\omega}}_{j-1}$ is the skew-symmetric matrix of $\boldsymbol{\omega}_{j-1}$, and in (4), $\boldsymbol{\omega}_{j-1,j}$ is the relative angular velocity between the bodies.

By following the principle of virtual power, Avello *et al.* [4] proposed that the virtual power of the forces acting on a multibody system can be written as

$$\delta\dot{\mathbf{q}}^{\mathrm{T}}\left(\mathbf{M}\ddot{\mathbf{q}} + \mathbf{C} - \mathbf{Q}\right) = 0 \tag{5}$$

where $\delta\dot{\mathbf{q}}$ are the virtual velocities of dimension $6N_b$; $\mathbf{M}$ is the diagonal mass matrix of the system; and $\ddot{\mathbf{q}} = \{\ddot{\mathbf{q}}_1^{\mathrm{T}}\ddot{\mathbf{q}}_2^{\mathrm{T}}\ldots\ddot{\mathbf{q}}_{N_b}^{\mathrm{T}}\}^{\mathrm{T}}$, $\mathbf{C} = \{\mathbf{C}_1^{\mathrm{T}}\mathbf{C}_2^{\mathrm{T}}\ldots\mathbf{C}_{N_b}^{\mathrm{T}}\}^{\mathrm{T}}$, and $\mathbf{Q} = \{\mathbf{Q}_1^{\mathrm{T}}\mathbf{Q}_2^{\mathrm{T}}\ldots\mathbf{Q}_{N_b}^{\mathrm{T}}\}^{\mathrm{T}}$ are vectors of dimension $6N_b$, where $\mathbf{C}$ denotes the quadratic velocity vector and $\mathbf{Q}$ denotes the external forces and torques. Note that the terms in parentheses in (5) represent the Newton–Euler balance of inertia and external forces and torques. In (5), the internal forces (the constraint forces) do not appear as they do not produce any virtual power for a kinematically admissible velocity. Consequently, the virtual velocities, $\delta\dot{\mathbf{q}}$, are assumed to be kinematically admissible, that is, they must satisfy the kinematic constraints. The virtual velocity vector $\delta\dot{\mathbf{q}}$ of dimension $6N_b$ can be expressed in terms of vector $\delta\dot{\mathbf{z}}$ of dimension $N_f$, where $N_f$ is the number of degrees of freedom of the system. Here, $\delta\dot{\mathbf{z}}$ are the virtual velocities of the joint coordinates. The velocity transformation matrix, $\mathbf{R}$, that relates the global coordinates and the relative joint coordinates, is introduced as follows

$$\dot{\mathbf{q}} = \mathbf{R}\dot{\mathbf{z}} \tag{6}$$

where $\dot{\mathbf{q}}$ is the generalized velocity vector and $\dot{\mathbf{z}}$ is the joint velocity vector. For scleronomic constraints (time independent), the kinematically admissible virtual velocities can be written as

$$\delta\dot{\mathbf{q}} = \mathbf{R}\delta\dot{\mathbf{z}}. \tag{7}$$

The acceleration equation can be expressed by taking the time derivatives of (6) as

$$\ddot{\mathbf{q}} = \mathbf{R}\ddot{\mathbf{z}} + \dot{\mathbf{R}}\dot{\mathbf{z}}. \tag{8}$$

By substituting (7) and (8) into (5), it can be expressed as

$$\delta\dot{\mathbf{z}}^{\mathrm{T}}\mathbf{R}^{\mathrm{T}}\left[\mathbf{M}\left(\mathbf{R}\ddot{\mathbf{z}} + \dot{\mathbf{R}}\dot{\mathbf{z}}\right) + \mathbf{C} - \mathbf{Q}\right] = 0. \tag{9}$$

As (9) holds true for any virtual velocity $\delta\dot{\mathbf{z}}^{\mathrm{T}}$, the virtual velocities can be eliminated and the equations of motion can be expressed as

$$\mathbf{R}^{\mathrm{T}}\mathbf{M}\mathbf{R}\ddot{\mathbf{z}} = \mathbf{R}^{\mathrm{T}}(\mathbf{Q} - \mathbf{C}) - \mathbf{R}^{\mathrm{T}}\mathbf{M}\dot{\mathbf{R}}\dot{\mathbf{z}} \tag{10}$$

which represents the $N_f$ number of ordinary differential equations of motion expressed in terms of relative joint coordinates. Note that the way the transformation matrix, $\mathbf{R}$ in (6), is computed plays an important role in the computational efficiency of this formulation. As explained in the literature, the analytical expression of the transformation matrix $\mathbf{R}$, obtained by using an element-by-element technique, is often the most efficient method [36]. The rows of $\mathbf{R}$ corresponding to the body $N_b$ are present in $\mathbf{R}_{N_b}$ once the zero columns are eliminated. The dimensions of $\mathbf{R}_{N_b}$ are $\left(6 \times N_{f\,b}\right)$, where $N_{f\,b}$ is the number of relative degrees of freedom found in the path that goes from the body $N_b$ to the ground. The matrix $\mathbf{R}_{N_b}$ can be expressed as

$$\mathbf{R}_{N_b} = \left[\mathbf{R}^1_{N_b}\mathbf{R}^2_{N_b}\ldots\mathbf{R}^{P_b}_{N_b}\right] \tag{11}$$

where $P_b$ is the number of joints in the path from the body $N_b$ to the ground. The size of each sub-matrix, $\mathbf{R}^i_{N_b}$, is $(6 \times D_i)$, where $D_i$ is the number of degrees of freedom of joint $i$. The expressions of matrix $\mathbf{R}^i_{N_b}$ for revolute, prismatic, cylindrical, universal, and spherical joint types are presented in [4].

For closed-loop systems, the equations of motion are derived by utilizing the cut-joint method and the penalty method as described by Bayo *et al.* [28]. Any closed-loop system can be expressed as an open-loop system (explained above) by simply cutting a joint in each kinematic loop and imposing the constraint conditions corresponding to the closure of the loops, as explained by Avello *et al.* [4].

### B. THE TERRAIN MODEL

The terrain/soil model used in this study is a combination of grid- and particle-based methods. By using the grid-based method, the soil model is defined as cells in a grid (a heightfield), in which each cell has properties, such as the position, stiffness, and friction. Fig. 2 represents the soil model in the static state. The method used here is particularly suitable for

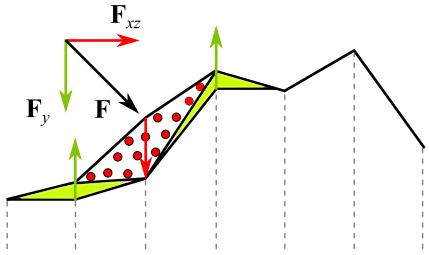


**FIGURE 3.** For a force $\mathbf{F}$ applied on the soil model, the vertical component $\mathbf{F}_y$ compresses and displaces the soil and the horizontal component $\mathbf{F}_{xz}$ generates the soil particles.

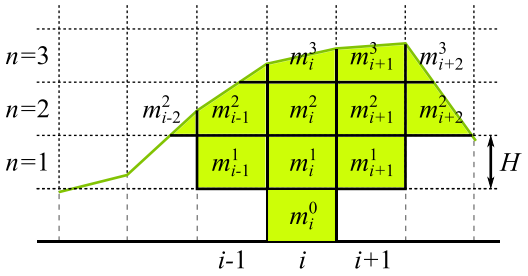


**FIGURE 4.** Uni dimensional automata are split into vertical slices to compute the pressure over the base of a cell.

fast collision detection and easy visualization. The vertical component of the force applied on the soil model compresses and displaces the soil, that is, it causes land compression and displacement, as shown in Fig. 3. By using the particle-based method, the soil can evolve and become unbound, which helps to describe the soil behavior. The horizontal component of the force applied on the soil model can generate the soil particles (see Fig. 3). When particles are generated, the grid height is updated based on the particles' volume. In this study, the particles have six degrees of freedom, containing both mass and inertia properties. Once the soil particles settle, they merge back to the heightfield with a volume update (that is, an accumulation of material on the ground).

### 1) SOIL GRID COMPRESSION AND DISPLACEMENT

In computer simulations, the evolution and visualization of the soil model's external surface is crucial. The cellular automata-based model [37], [38] is simple and it describes the soil model as cells in a grid (a heightfield) so that it can be efficiently rendered by graphics processors. The main advantage of a cellular automata model is that it can be executed in real time and it can be managed in a three-dimensional graphics environment. The system is assumed to having a constant density condition, that is, a cohesionless material forms a system with low compressibility, such as, dry sand.

Cellular automata on an $L \times L$ square grid are considered, where the variable $h(i, j)$ is the height of the system at the center of the cell $(i, j)$. To compute the pressure over the base of one cell, the automata are split in vertical slices so that the material over a cell can be considered as a pile of blocks of height $H$. For simplicity, Fig. 4 shows such a representation of uni dimensional automata, where $p_i^n$ and $m_i^n$ are, respectively, the total pressure at the base and the weight of the $n^{th}$ block located over the $i^{th}$ cell. The pressure over the base of a cell is calculated by considering the pressure by their own block and the pressure received by a finite number of the closest blocks in the upper level, all of them centered over the $(i, j)$ cell. The propagation of pressure from the layer $n$ blocks to layer $(n-1)$ is expressed by means of a symmetric function $\phi$ so that

$$\left.\begin{aligned} \phi(k) = 0 \quad \forall k : |k| > 1 \\ \phi(-1) + \phi(0) + \phi(1) = 1 \end{aligned}\right\} \tag{12}$$

where $\phi(t)$ is the rate of the pressure received by the base of block $i$ in layer $n$ that is propagated to block $(i + t)$ in layer $(n - 1)$. For real-time applications, the total weight/pressure over the base of the $(i, j)$ cell can be written as

$$p_{ij}^0 = \sum_{n=0}^{N} \sum_{s=-n}^{n} \sum_{t=-n}^{n} a_{stn} m_{i+sj+t}^n \tag{13}$$

where

$$\left.\begin{aligned} a_{stn} = \sum_{k_1+\cdots+k_n=s} \sum_{l_1+\cdots+l_n=t} \phi^{k_1 l_1} \cdots \phi^{k_n l_n} \\ a_{000} = 1 \end{aligned}\right\} \tag{14}$$

where $\phi^i$ is used to denote $\phi(i)$. This leads to an efficient pressure distribution update. Note that in the presence of an external force, it is only required to add the equivalent weight to the block where the force is applied. Equation (13) only depends on the state of the cellular automata model, therefore, it can be applied to the interactive cellular automata model described below.

During soil deformation, which results from the object and soil grid interaction at some point, the previously untouched terrain in the immediate vicinity (the soil grid region) is subjected to another type of deformation, such as macroscopic patterns or avalanches. The formation of macroscopic patterns or avalanches can be modeled using cellular automata [37], [38]. In the used cellular automata model, the displacement of material (soil) can be triggered both by a large difference in height and by a large difference between the vertical forces applied to two neighboring cells.

Again, cellular automata on an $L \times L$ square grid are considered, where the variable $h(i, j)$ is the height of the system at the center of the cell $(i, j)$. Let the scalar value of the applied vertical force on each cell be $f(i, j)$ and let $F$ be a real function so that $F : IR \rightarrow IR$. Two new variables are introduced: $h_f$ as the composition $h_f(i, j) = F(f(i, j))$, and the sum $h' = h + h_f$. A parameter $\alpha$ is introduced, which is the friction angle (the piling slope) of the system in order to simply constrain material change between the adjacent cells. In the simulation, if the calculated slope angle is smaller than the defined friction angle (the piling slope), then the material is not moved between cells without the application of external pressing force. In this study, the internal friction angle is

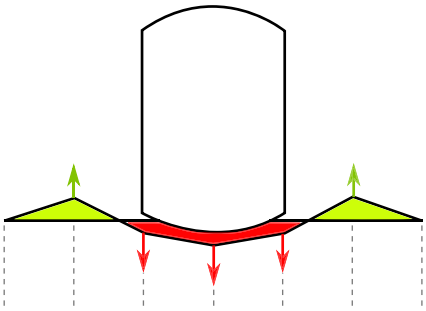

**FIGURE 5.** Soil compression and displacement.

considered 35°. For each cell $(i, j)$, $\nabla h'$ is computed. For the cells where $\arctan\left(\left|\nabla h'\right|\right) > \alpha$, the automata state can be updated as follows (pictorially represented in Fig. 5)

$$\left.\begin{aligned} h(i,j) &\leftarrow h(i,j) - z_+ \cdot (h'_x(i,j) + h'_y(i,j)) \\ h(i+1,j) &\leftarrow h(i+1,j) + z_+ \cdot h'_x(i,j) \\ h(i,j+1) &\leftarrow h(i,j+1) + z_+ \cdot h'_y(i,j) \end{aligned}\right\} \quad (15)$$

where $z_+$ is the velocity of the flowing matter, and $h'_x$ and $h'_y$ are the approximations to the partial derivative of $h'(x, y)$. The function $F$ is approximated to be the height of a square column of material that weighs exactly $f$, as shown below

$$F(f) = \eta \frac{f}{d^2 \rho g} \quad (16)$$

where $g$ is the acceleration due to gravity, $\rho$ is the density of the material, $d^2$ is the area of the cell of the automata, and $\eta > 0$ is a parameter that allows defining how easily the force can cause the matter to be displaced. The force function $F$ defined in (16) can integrate well with contact force models based on spring-damper equations (explained in Section II-D). The parameter $\eta$ is determined based on the computation time of the simulation model in each iteration (such as the defined time step) and the amount of material that is moved between the cells. If $\eta = 0$ then there is no transfer of material between the cells. In this study, the value of $\eta$ is assumed to be 4.

In this study, the parameter tuning for a given set of terrain properties is carried out case by case. This is due to the fact that the parameters are dependent on the complexity of the structure/machine and the collision geometries. The parameters are cumbersome to relate to the parameters that are usually employed to characterize soil behavior, such as the terrain cohesion or the pressure-sinkage coefficients in terramechanics models. The cellular automata-based model is consistent with actual terrain behavior. In [37], it is shown that the evolution of the surface of the cellular automata-based model is similar to the BCRE model presented by Bouchaud *et al.* [39]. Accordingly, the used cellular automata model provides a realistic and a computationally inexpensive model.

#### 2) SOIL PARTICLE GENERATION AND REPRESENTATION

Soil particle generation is a force-based phenomenon. As shown in Fig. 3, when the horizontal component, $\mathbf{F}_{xz}$, of the force applied on the soil model is greater than the shear impulse limit, it generates soil particles. Soil failure is modeled by substituting the corresponding heightfield (static soil column) portion with soil particles, and consequently, the heightfield is lowered.

The granular soil particles are represented/simulated as rigid spherical bodies with six degrees of freedom. Their equations of motion are described by using the multibody formulation described in Section II-A. The rotations of the rigid spherical bodies are defined by using Euler parameters. In this study, all the friction is described by using the LuGre model for sliding (explained in Section II-D). The material properties — such as the contact spring and restitution coefficient, coefficient of sliding friction (friction coefficient), mass and moment of inertia of one particle system, and translational and rotational damping for the rigid spherical bodies — are introduced manually. In the soil particle representation, the degree of soil compaction (the packing of soil particles) is considered by assigning a void ratio value to all the free particles that is updated with each simulation step. This allows the soil to be represented as it appears in nature, where the overall volume of the soil is formed by its voids rather than solids. The consideration of the void ratio at the position of the soil particle allows the total volume transfer of the particle to the soil grid when the particles reach equilibrium and are merged into the soil grid (explained in Section II-B.3). This approach has a significant impact on the visual representation of the simulated soil particles.

To keep the real-time criteria, the size of the granular soil particles is determined based on the limit for the number of particles. The limit for the number of particles is determined by the complexity of the structure/machine, which includes the geometry of collision. In this study, the number of particles are limited to a maximum of 1000 particles in the bucket at a time.

#### 3) SOIL PARTICLE MERGING

On reaching equilibrium (that is, the linear and angular velocity is below the threshold value), the soil particles that are in contact with the soil grid do not contribute to the soil dynamics. In such a situation, the soil particles are removed from the simulation and are replaced with a static volume in the soil grid by increasing the corresponding heightfield (the soil columns' height). Here, an interpolated filter kernel is applied to preserve the volume. This approach helps to achieve a real-time simulation capability by considerably reducing the total number of soil particles without affecting the soil dynamics' behavior.

### C. HYDRAULIC ACTUATOR MODELING

In this study, lumped fluid theory [5] is used to describe the hydraulic pressures within a hydraulic circuit. In this method, the hydraulic circuit is partitioned into discrete volumes where the pressure is assumed to be evenly distributed. In practice, the effect of acoustic waves is assumed to be insignificant. The pressure build up (the first derivative of

pressure, $p_s$) within each hydraulic section of volume, $V_s$, can be written as

$$\dot{p}_s = \frac{B_{e_s}}{V_s} \sum_{k=1}^{n_c} Q_{sk} \tag{17}$$

where $Q_{sk}$ is the sum of the incoming and outgoing flow in/out of a node (that is, the volume $V_s$), $n_c$ is the total number of hydraulic components related to the volume $V_s$, and $B_{e_s}$ is the effective bulk modulus of the hydraulic section of the volume $V_s$. A semi-empirical approach [40] can be used to model valves that are used to control the pressure difference, the flow rate, and the direction of flow. In this approach, the flow rate through a valve, $Q$, can be expressed as

$$Q = C_v U \sqrt{dp} \tag{18}$$

where $C_v$ is the semi-empirical flow rate constant of the valve (which in many cases, such as with directional valves, can be obtained from manufacturer catalogues), $dp$ is the pressure difference over the valve, and $U$ is the relative spool/poppet position that can be expressed by using the first order equation as

$$\dot{U} = \frac{U_{ref} - U}{\tau} \tag{19}$$

where $U_{ref}$ is the reference voltage signal for the reference spool/poppet position and $\tau$ is a time constant that can be read from the Bode diagram of the valve, describing the valve spool/poppet dynamics.

### D. CONTACT AND TIRE MODELING

In multibody systems, the function of a contact model is to prohibit the inter-penetration of bodies. In practice, there are two steps in contact modeling: collision detection and collision response [41]. The collision between bodies is detected by using a bounding volume approach, which utilizes simple bounding volumes, such as spheres and boxes, to enclose bodies with complex geometries. In this study, the collision detection is determined by employing the object-oriented bounding box method [32]. This method uses a minimum rectangular solid to enclose the body along the direction of the axis. Fig. 6a illustrates this collision detection method in two dimensions between two bodies $B_{j-1}$ and $B_j$ that are enclosed in boxes E and F respectively. The two boxes do not overlap if the following condition is met, as shown below

$$\mathbf{T} \cdot \mathbf{L}_i > d_{Ei} + d_{Fi} \tag{20}$$

with,

$$d_{Ei} = e_1\mathbf{E}_1 \cdot \mathbf{L}_i + e_2\mathbf{E}_2 \cdot \mathbf{L}_i \tag{21}$$

$$d_{Fi} = f_1\mathbf{F}_1 \cdot \mathbf{L}_i + f_2\mathbf{F}_2 \cdot \mathbf{L}_i \tag{22}$$

where $|\mathbf{T}|$ is the distance between the centres of boxes E and F; $\mathbf{L}_i$ is a normalized direction; $e_1$ and $e_2$ are the dimensions of box E; $f_1$ and $f_2$ are the dimensions of box F; $\mathbf{E}_1$ and $\mathbf{E}_2$ are the normalized axes of box E; and $\mathbf{F}_1$ and $\mathbf{F}_2$ are the normalized axes of box F. In three dimensions, the boxes do not overlap if (20) holds true for all 15 potential separating axes, that is, $i = 1 : 15$.

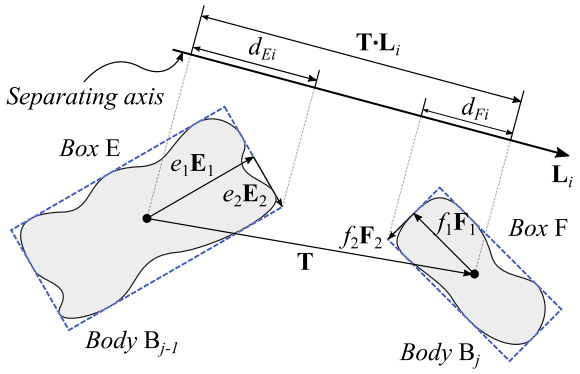


(a) Collision detection using the object-oriented bounding box method.

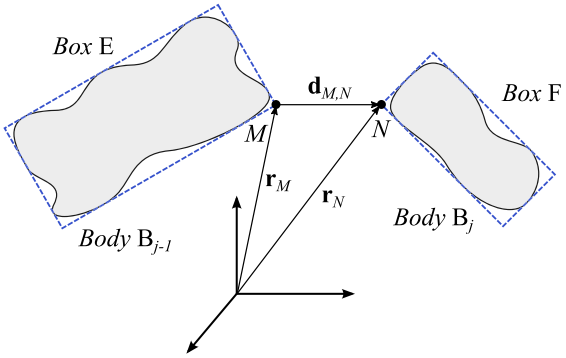


(b) Collision response using the penalty method.

**FIGURE 6. Contact modeling consists of collision detection and collision response.**

In practice, the contact description based on the penalty method [33] is computationally efficient enough that it can be used in a real-time application. In this study, the geometry-based model (the single collision point model) is used to determine the contact force (the collision response) between the bodies involved. From Fig. 6b, the magnitude of the relative displacement, $\mathbf{d}_{M,N}$, and relative velocity, $\dot{\mathbf{d}}_{M,N}$, between the collision points $M$ and $N$ along the collision normal is derived (as in Section II-A) in the global reference frame as

$$\left|\mathbf{d}_{M,N}\right| = (\mathbf{r}_N - \mathbf{r}_M) \cdot \mathbf{n} \tag{23}$$

$$\left|\dot{\mathbf{d}}_{M,N}\right| = (\dot{\mathbf{r}}_N - \dot{\mathbf{r}}_M) \cdot \mathbf{n} \tag{24}$$

where $\mathbf{n} = \frac{(\mathbf{r}_N - \mathbf{r}_M)}{|(\mathbf{r}_N - \mathbf{r}_M)|}$ is the normal vector of the collision; $\mathbf{r}_M$ and $\mathbf{r}_N$ are, respectively, the position of collision points $M$ and $N$ with respect to the global reference frame; and $\dot{\mathbf{r}}_M$ and $\dot{\mathbf{r}}_N$ are their respective velocities in the global reference frame. The normal contact force, $\mathbf{F}_n$, at the collision point can be written as

$$\mathbf{F}_n = -\left(K\left|\mathbf{d}_{M,N}\right| + C\left|\dot{\mathbf{d}}_{M,N}\right|\right)\mathbf{n} \tag{25}$$

where $\left|\mathbf{d}_{M,N}\right|$ becomes the penetration distance at the contact point, $K$ is the coefficient of elasticity, and $C$ is the damping factor.

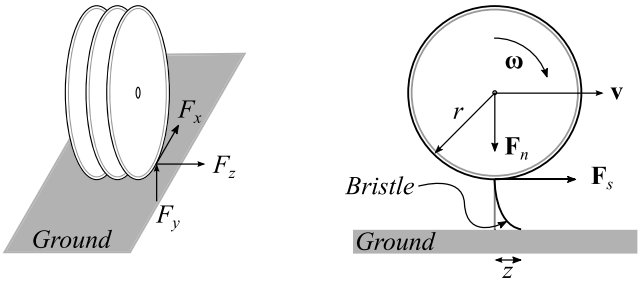


**FIGURE 7.** The lumped LuGre tire model.

In tire modeling, the tires are presumed to be a series of discs, as shown in Fig. 7 (on the left), where the typical forces involved are the longitudinal force $F_x$, lateral force $F_z$, and vertical force $F_y$. To meet the real-time criterion for this study, a tire is described by using the lumped LuGre tire model [34], [35], as shown in Fig. 7 (on the right). The approach can be seen as an extension of the Dahl model as it includes the Stribeck effect. It assumes punctual tire–ground friction contact. The lumped LuGre model proposed by De Wit *et al.* [34] can be written as

$$\dot{z} = |\mathbf{v}_r| - \frac{\sigma_0 |\mathbf{v}_r|}{g(\mathbf{v}_r)} z \tag{26}$$

$$|\mathbf{F}_s| = (\sigma_0 z + \sigma_1 \dot{z} + \sigma_2 |\mathbf{v}_r|)\, |\mathbf{F}_n| \tag{27}$$

with,

$$g(\mathbf{v}_r) = \mu_c + (\mu_s - \mu_c)\, e^{-\left|\frac{\mathbf{v}_r}{\mathbf{v}_s}\right|^{\frac{1}{2}}} \tag{28}$$

where $\sigma_0$ is the rubber longitudinal lumped stiffness, $\sigma_1$ is the rubber longitudinal lumped damping, $\sigma_2$ is the viscous relative damping, $\mu_c$ is the normalized Coulomb friction, $\mu_s$ is the normalized static friction ($\mu_c \leq \mu_s \in [0, 1]$), $\mathbf{v}_s$ is the Stribeck relative velocity, $\mathbf{F}_s$ is the friction force based on bristle deformation, $\mathbf{F}_n$ is the normal force, $z$ is the deflection of the bristles (the internal friction state), and $|\mathbf{v}_r| = r\,|\boldsymbol{\omega}| - |\mathbf{v}|$ is the magnitude of the relative velocity, where $r$ is the tire radius, and $\boldsymbol{\omega}$ and $\mathbf{v}$ are, respectively, the angular and linear velocity of the tire. In practice, (26) is solved by using the time integration scheme (the trapezoidal method). One of the limitations associated with this tire modeling technique is that the tire properties are assumed to be identical in the longitudinal and lateral directions. This is not the case in practice. Another limitation is that this tire model is based on a simplified LuGre model. In this study, a tire is modeled by using a series of discs while the contact patch, as predicted by a deformable tire model, is not considered. Therefore, the abrupt change in the normal contact pressure and slip distributions over the contact patch caused by the large load transfer are not considered in this tire model.

Regarding the transmission of forces between the vehicle and the terrain, in every iteration, the contact forces between the wheel and the ground are evaluated first. Then, the shape of the terrain model (explained in Section II-B) is updated based on the forces applied to the deformable terrain. Note that in the next iteration, the contact forces are re-evaluated based on the updated soil shape. Accordingly, the soil model is deformed continuously during the vehicle and terrain interaction. Prior to the evaluation of the contact forces between the wheel and the ground, the terrain is represented as static volumes in the soil grid, that is, it is considered rigid.

## III. A CASE STUDY OF A HYDRAULICALLY ACTUATED TRACTOR MODEL

In this study, the tractor model shown in Fig. 8 is demonstrated as a case example. The tractor is modeled by using the semi-recursive approach, as explained in Section II-A. Fig. 8 demonstrates the connecting components of the tractor model, and the model structure is summarized in Table 1. There are eight revolute joints, three spherical joints, two universal joints, and two fixed joints, as shown in Fig. 8. The structure consists of open-loop and closed-loop links. For the closed-loop links, three cut joints are introduced at three revolute joints (marked in Fig. 8) and 15 closed-loop constraint equations are introduced for the closure of the loops. The system has nine degrees of freedom, with six degrees of freedom corresponding to the three translational and three rotational axes of the tractor, one degree of freedom corresponding to the steering mechanism, and two degrees of freedom corresponding to the lift and tilt rotational axes of the front-loader.

**TABLE 1.** Summary of the tractor model structure.

| Name | Number |
|---|---|
| Number of bodies | 13 |
| Number of joints | 15 |
| Number of joint coordinates | 28 |
| Number of closed-loop constraint equations | 15 |
| Degrees of freedom | 9 |

The front-loader of the tractor is operated by using hydraulic actuators. As the tractor model under consideration is subjected to product development and other product processes, a simplified version of the actual hydraulic circuit for the front-loader is utilized, as shown in Fig. 9. The circuit consists of a fixed displacement pump, two 4/3 directional control valves, and four double-acting hydraulic cylinders. The control volumes ($V_P$, $V_1$, $V_2$, $V_3$, and $V_4$) used in modeling the hydraulic circuit are also marked in Fig. 9. For the sake of simplicity, the circuit is assumed to be ideal, that is, leakage is not considered.

A deformable sand field is simulated by using the heightfield-based algorithm introduced in Section II-B. The dynamic performance of the tractor on this deformable sand field is analyzed when it lifts a bucket of sand from a pile of sand and dumps it in another place on the deformable ground (the sand field). This sand field model allows the correct bucket-filling process, both visually and physically (as shown in Fig. 10), that is, the bucket is filled by using the

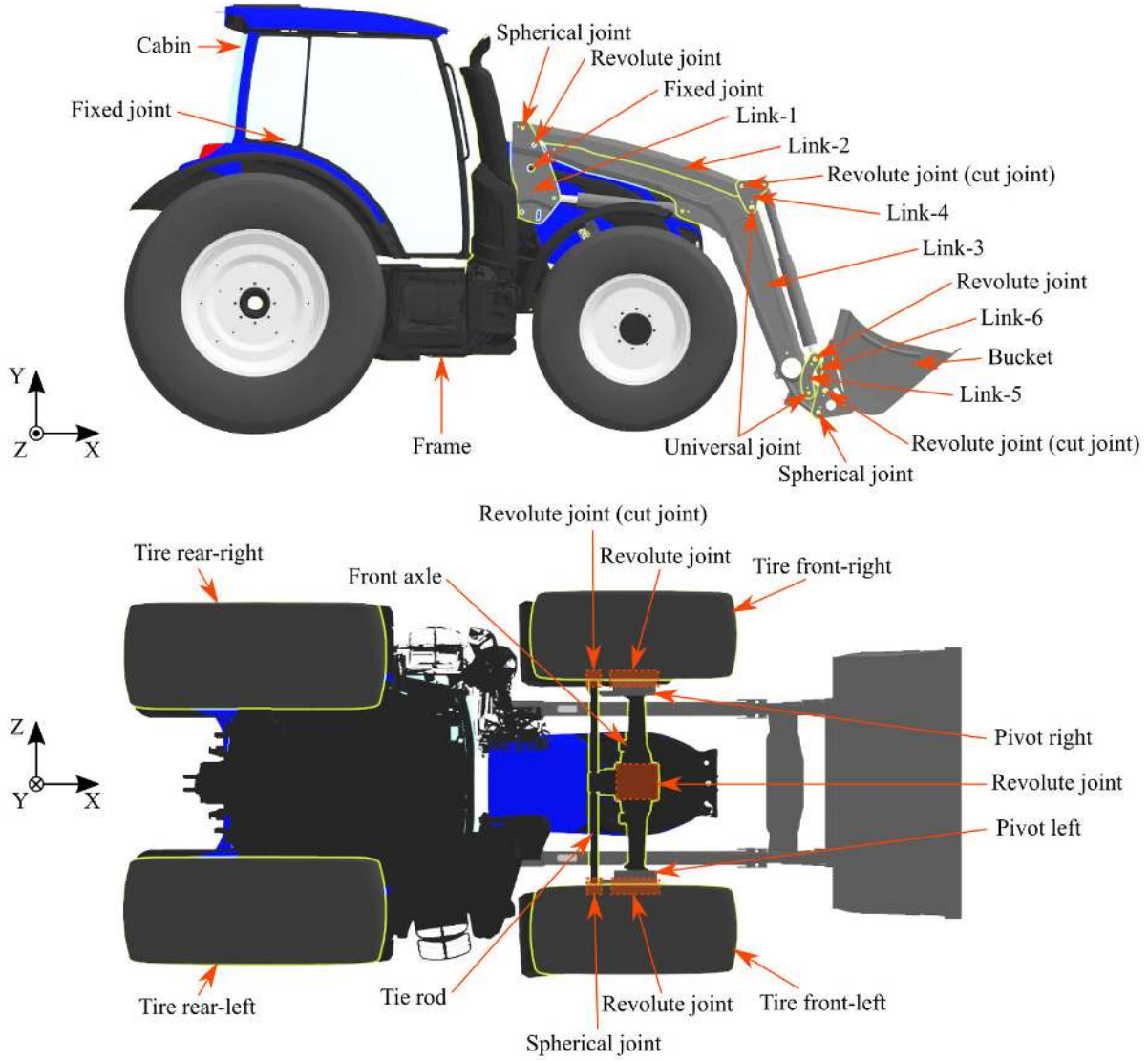


**FIGURE 8.** Connecting components in the tractor simulation model.

physically correct mass particles. By using the force points in the bucket, which are defined in the collision graphics of the bucket, the force at each force point is calculated independently. For the nearest cell to each force point, the direction, magnitude, and cutting force between the cells and force points are evaluated. When the cutting force reaches the penetration limit for the heightfield, particles are generated. Note that the forces at various force points on the bucket cause an uneven force distribution on the bucket, resulting in a load and moment to the structure. This study is concerned with a maximum of 1000 particles in the bucket at a time, as mentioned in Section II-B.2. Note that as the size of the particles is dependent on a number of parameters (such as the number of particles, complexity of the structure/machine, and collision geometries), the simulation result is only obtained for one kind of particle size. The size of these particles is not varied within the scope of this paper.

The nature of the terrain model introduced in this study is such that it is spatially independent, that is, the terrain in one area is independent of the terrain in another area. This implies that the computation of different areas of the terrain can be done in parallel. It does not depend on when/where the computations of different areas are performed as long as the computations are all completed before moving on to the next set of calculations. The multibody and hydraulics models are coupled, that is, a monolithic approach is used. The tractor simulation model used in this study is complex as it involves small time steps (0.0012 s), the use of hydraulics, and interaction with particle systems (in the terrain/soil model). The details about the operating system, processor, random access memory, graphics memory, and display adapter with which the simulation is performed are mentioned in Table 2. The tractor model is simulated in a C++ environment (compiler: Microsoft Visual Studio, version 14.1).

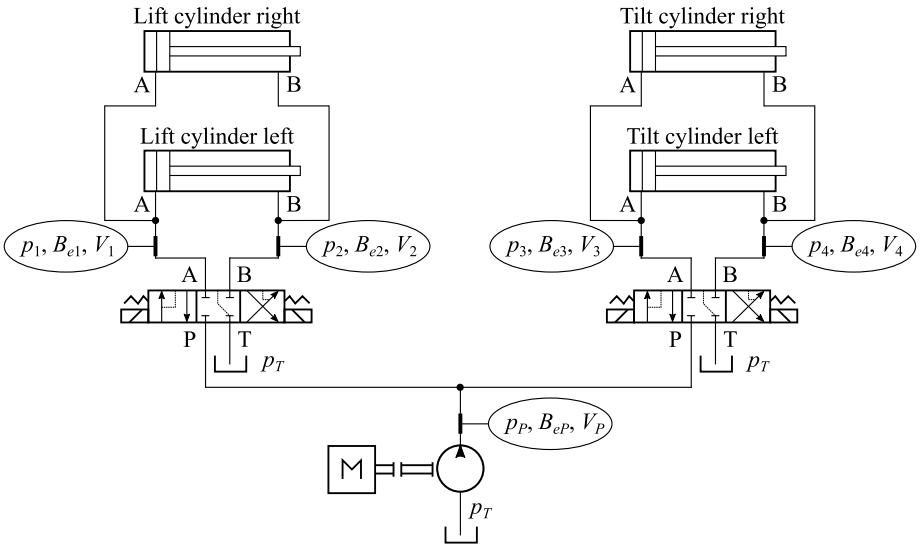


**FIGURE 9.** The front loader's hydraulic system.

**TABLE 2.** A description of the computer used for the simulation.

| Name | System used |
|---|---|
| Operating system | Windows 10 |
| Processor | Intel Core i7 3.41 GHz |
| Random access memory | 64.0 GB |
| Graphics memory | 36809 MB |
| Display adapter | Nvidia Quadro M2000 |

## IV. RESULTS AND DISCUSSION

This section presents the simulation results of the real-time tractor on the deformable sand field. Fig. 10 shows simulation frames of the tractor model at different instants of time. In this study, the work cycle of the tractor model follows a 3D maneuver that is used to load the bucket with an amount of sand from a pile of sand and then dump it in another place on the deformable ground (the sand field). Here, the real-time capability of the system (the tractor simulation model) is analyzed. The performance of the soil/terrain model is compared with the multibody and hydraulics model, and their real-time capability is determined. The dynamic actuator forces in the hydraulic cylinders are compared with the static actuator forces (computed analytically) for the digging and dumping operation. The pressures in the hydraulic cylinders are also studied.

### A. THE WORK CYCLE (THE 3D MANEUVER)

In this study, the tractor model follows a 3D maneuver, as shown in Fig. 11. At the beginning, the tractor is released from a height of 0.3 m at time 0.00 s. Then, the bucket is lifted-up (1.52 s to 2.36 s) and tilted outwards (2.96 s to 4.10 s) to the desired height and angle for the bucket to carry out the digging operation. Next, the tractor is driven forward (4.88 s

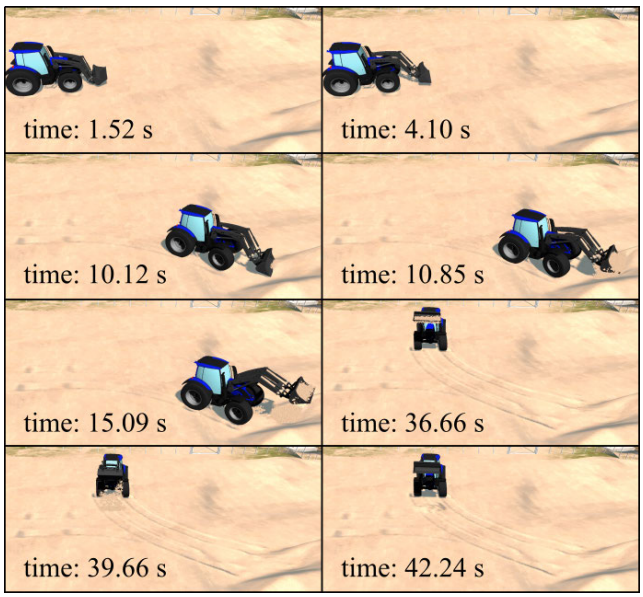


**FIGURE 10.** Simulation frames of the tractor model at different instants of time.

to 10.81 s) towards a pile of sand along the curvature shown in Fig. 11. Note that the ground is not a flat plane, but has an undulating surface. Meanwhile, the bucket makes contact with the pile of sand at 10.12 s, digs an amount of sand until 10.85 s, and then the tractor is brought to a stop. During the collision between the bucket and the static sand field (the deformable ground), the static sand is converted into granular sand particles (10.12 s to 10.85 s). Next, the bucket is lifted up (10.56 s to 12.41 s) and slightly tilted inwards (10.32 s to 11.96 s) in order to fill the bucket with sand particles. Then, the tractor is driven in reverse (15.09 s to 34.60 s) along the curvature shown in Fig. 11. During reversing, the angle of

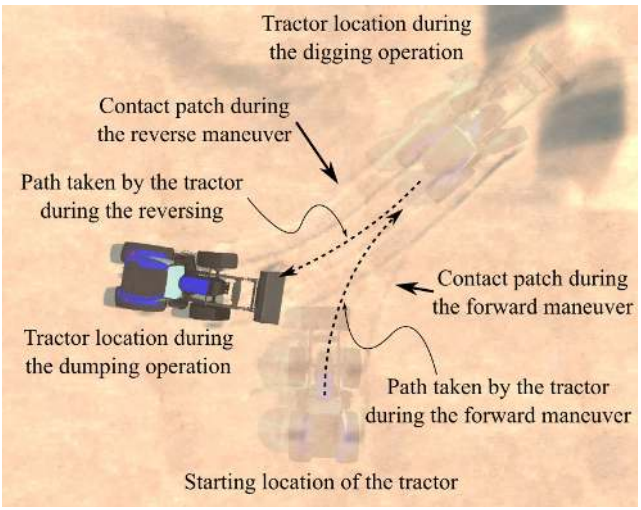


**FIGURE 11.** 3D maneuver of the tractor simulation model.

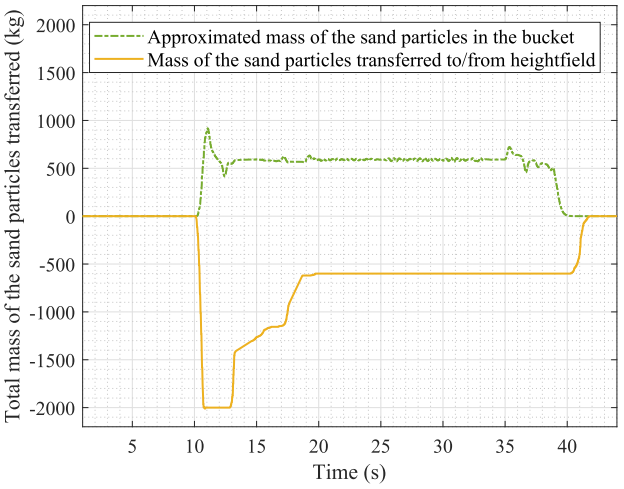


**FIGURE 12.** Total mass of the sand particles transferred during the simulation.

the bucket is slightly adjusted by tilting the bucket inwards (16.78 s to 17.42 s). Note that as the tires compress the soil/terrain model during the forward/backward maneuver, they make a contact patch on the undulating deformable ground, as shown in Fig. 11. Next, the tractor is brought to a stop, and the sand-filled bucket is raised (34.88 s to 36.66 s) and tilted outwards (35.00 s to 39.66 s) in order to dump the sand particles back on the ground. At last, the empty bucket is tilted inwards (40.78 s to 42.24 s) to complete the simulation process.

### B. THE COLLECTION OF SAND PARTICLES

During the loading and transfer of the sand particles, the amount of sand being dug and collected in the bucket is shown in Fig. 12. During the digging operation (10.12 s to 10.85 s), the static sand field is converted into sand particles. The mass of sand particles inside the bucket before the digging (0 s to 10.12 s) and after the dumping operation (41.78 s to 44 s) is zero. Between 10.85 s to 12.85 s, the bucket is filled with approximately 600 kg of sand. Between 12.85 s to 19.72 s, the sand particles that are not collected in the bucket merge back into the sand field on reaching an equilibrium state, as mentioned in Section II-B.3. During the reversing of the tractor (15.09 s to 34.60 s), care is taken so that the sand particles are not dropped from the bucket. Note that the mass in the bucket is detected using a mass sensor. The mass sensor approximates the mass based on the number of sand particles crossing a specific location (inside the bucket) near the teeth of the bucket. The mass in the bucket (between 12.85 s to 37.20 s) slightly fluctuates around 600 kg because of tiny movements of the bucket caused by either the hydraulic actuators or the tractor's movement. Furthermore, the peaks in the curve depicting the approximated mass of the sand particles in the bucket, see between 10.50 s and 13 s and between 35 s and 38 s, should be noted. These are caused because of a sudden tilt/lift of the bucket causing the mass sensor to detect either some extra particles crossing the bucket or a loss of particles as they lose contact with the bucket. The moment the sand particles in the bucket are dumped (37.20 s to 40.28 s), they are merged back into the static sand field (40.28 s to 41.78 s) on reaching an equilibrium state.

### C. REAL-TIME CAPABILITY

The tractor simulation model presented in this study is real-time capable, that is, the computation is synchronized to real time. For the presented work cycle, Fig. 13 represents the loop duration of the tractor simulation model. For the entire work cycle, the loop duration is always less than the time step (0.0012 s) of the simulation model. Therefore, the tractor simulation model is clearly real-time enabled. Note that from the time the sand particles are generated (10.12 s) until the time when they are merged back into the static sand field (41.78 s), the loop duration is higher in comparison with when no particles are generated/present.

For the work cycle presented above, the performance (measured in terms of integration time) of the soil/terrain model in comparison to the performance of the multibody and hydraulics model is shown in Fig. 13. Note that as mentioned in Section III, a monolithic approach is used for the multibody and hydraulics model. The integration time (the actual computation time) of the multibody and hydraulics model always fluctuates between 0.26 ms to 0.43 ms throughout the presented work cycle; whereas for the soil/terrain model, it varies depending upon the compression of the sand field and the generation/handling of the sand particles. As shown in Fig. 13, the integration time of the soil/terrain model is relatively low when no particles are present. At those instances, the soil/terrain model only undergoes compression because of the tires of the tractor. Otherwise, the integration time is relatively high from the moment the sand particles are generated/present. Furthermore, the integration time of the soil model depends on the number of sand particles

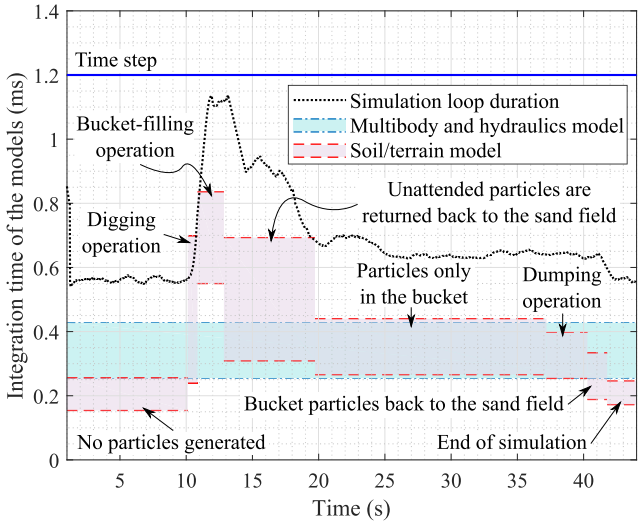


**FIGURE 13.** Performances of the models with respect to the simulation run time.

present/generated. A large number of sand particles results in a higher integration time. In conclusion, when no particles are generated/present, the integration time of the soil model is lower than the multibody and hydraulics model. Otherwise, the integration time of the soil model is higher, depending upon the number of sand particles generated/present and their handling. For the soil/terrain model and the multibody and hydraulics model, the integration time is always less than the time step (0.0012 s).

### *D. ACTUATOR FORCE AND HYDRAULIC PRESSURE IN THE HYDRAULIC CYLINDERS*

This study introduced a real-time capable, deformable terrain/soil model that can interact with the dynamics of the hydraulics model along with the multibody dynamic system. Therefore, it becomes necessary to provide simulation results for the hydraulic pressure and actuator force in the hydraulic cylinders for the presented work cycle. The analysis is focused on the duration between the digging and dumping operations, that is, when the sand particles are generated/present. Such simulation results can be utilized in product development and other product processes. In the hydraulics subsystem, 4/3 directional control valves for the lift and tilt operations are modeled as an input signal for the user. For the lift operation, Fig. 14 represents the response of the hydraulics subsystem when the bucket loads and transfers approximately 600 kg of sand from a deformable ground area (the sand field). As per the presented work cycle, the important regions on the plots in Fig. 14 are highlighted in purple for the lift operation.

During the lift operation, the hydraulic pressure across the right/left hydraulic lift cylinder is shown in Fig. 14a. The actuator forces of the lift cylinders (right and left) are shown in Fig. 14b. The right and left lift cylinders have identical dynamic actuator forces. Therefore, the pressure plot is

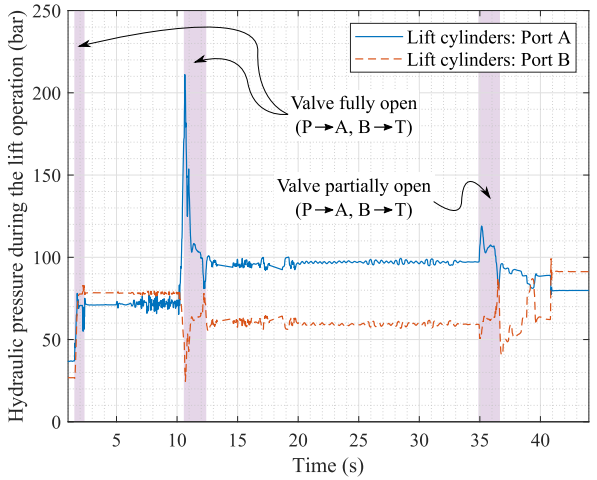


(a) Hydraulic pressure across the hydraulic lift cylinders during the lift operation.

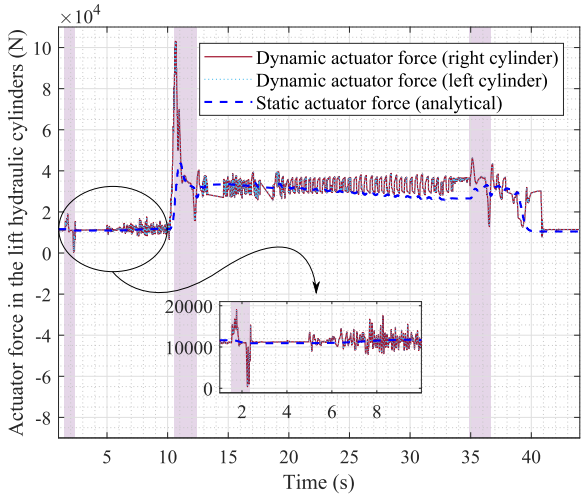


(b) Actuator forces in the hydraulic lift cylinders during the lift operation.

**FIGURE 14.** Simulation results for the front-loader's hydraulic lift cylinders during the lift operation.

shown for only one of the lift cylinders. Between 10.12 s and 10.85 s, a high order (of the order 100 kN), fluctuating, dynamic actuator force occurs, representing the collision of the bucket with the static sand field. During this period, a peak fluctuation in the pressure plot is also observed. The collision of the bucket with a pile of sand is a harsh operation. When the bucket is filled with sand particles (10.85 s to 37.20 s), more pressure is applied on the piston side (port A) compared with the piston-rod side (port B) (see Fig. 14a). As a result, more actuator force is applied to support the extra weight of the sand particles, as can be seen in Fig. 14b. Between 10.85 s and 37.20 s, the pressure in the lift cylinder and the dynamic actuator force fluctuates because of the mass fluctuation in the bucket. The dynamic actuator force in the lift cylinder is compared with its static actuator force, which is analytically computed without considering the dynamics of the system. It can be concluded that the dynamic actuator force showed good agreement with the static actuator force. A similar

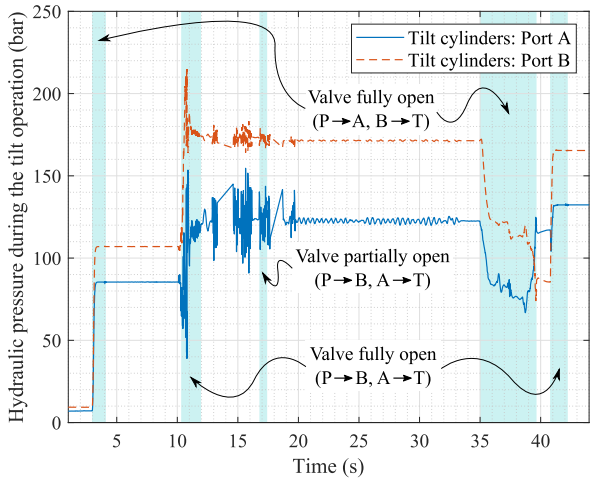


(a) Hydraulic pressure across the hydraulic tilt cylinders during the tilt operation.

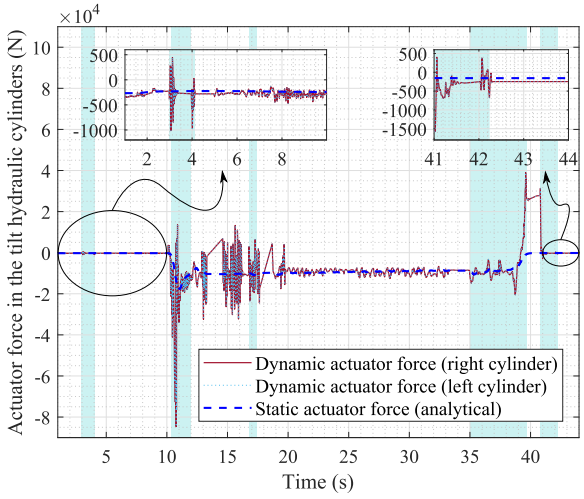


(b) Actuator forces in the hydraulic tilt cylinders during the tilt operation.

**FIGURE 15. Simulation results for the front-loader's hydraulic tilt cylinders during the tilt operation.**

analysis can be carried out for the tilt operation (Fig. 15) where the important regions on the plots are highlighted in cyan for the tilt operation.

## V. CONCLUSION

This study demonstrated a real-time simulation approach that consists of a unique combination of multibody formulation, hydraulic actuators, and a deformable terrain/soil model. The introduced approach is ideal for the real-time analysis of the dynamics of a complex mobile machine. As a case study, a tractor was modeled by using a semi-recursive multibody formulation based on velocity transformation. A deformable sand field (the ground) was modeled by combining a mesh-based and particle-based soil representation method for the real-time simulation of soil deformation. The hydraulic actuation of the tractor's front-loader was modeled by utilizing the lumped fluid theory.

This study presented the dynamic behavior of the tractor work cycle in which the tractor dug an amount of sand from a pile of sand and dumped it in another place on a deformable ground area (the sand field). The work cycle of the tractor model followed a 3D maneuver. During the 3D maneuver, the tires made a contact patch on the undulating deformable ground as they compressed the soil/terrain model. During the digging operation, the static sand field was converted into sand particles and these were collected in the bucket of the tractor. During the dumping operation, the sand particles merged back into the static sand field on reaching an equilibrium state.

The tractor model was real-time capable as the loop duration was always less than the time step. The loop duration was higher when the sand particles were generated/present in comparison with when no particles were generated/present. This was caused by the fact that the integration time of the soil/terrain model was higher, which was dependent on the number of sand particles generated/present and their handling. In other situations, the integration time of the soil/terrain model was lower than the multibody and hydraulics model, which followed a monolithic approach. The soil/terrain model and the multibody and hydraulics model were real-time capable.

The simulated bucket and sand pile collision caused a high order fluctuating actuator force (dynamic) and a peak fluctuation in the pressure, demonstrating a similarly harsh operation as it would be in practice. When the bucket was filled with sand particles, more pressure was applied on the piston side compared to the piston-rod side (the lift cylinders), resulting in more dynamic actuator force (from the lift cylinders) to support the extra weight of the sand particles. The dynamic actuator force showed good agreement with the static actuator force. Such a real-time capable tractor simulation model can be utilized in product development and other product processes.

It should be noted that due to the lack of experimental data, no thorough validation regarding the accuracy of the tractor simulation model was provided. The validation for the physical correctness of the cellular automata model was already provided in the literature [37]. Furthermore, it has been carefully checked that the modeled tractor behaved in a logical manner. It is also worth noting that the results obtained from the hydraulics subsystem of the tractor model showed good agreement when compared to simple analytical models. This study provided a conceptual-level implementation of a possible simulation model that is focused on the entire environment.

## REFERENCES

[1] M. Blundell and D. Harty, *The Multibody Systems Approach to Vehicle Dynamics*. Oxford, U.K.: Butterworth-Heinemann, 2015.

[2] G. Panetta, F. Mancarella, M. Borghi, B. Zardin, and F. Pintore, "Dynamic modelling of an off-road vehicle for the design of a semi-active, hydropneumatic spring-damper system," in *Proc. ASME Int. Mech. Eng. Congr. Expo.*, Houston, TX, USA, 2015, pp. 1–11.

[3] M. E. Baharudin, A. Rouvinen, P. Korkealaakso, and A. Mikkola, "Real-time multibody application for tree harvester truck simulator," *Proc. Inst. Mech. Eng. K, J. Multi-Body Dyn.*, vol. 228, no. 2, pp. 182–198, 2014.

[4] A. Avello, J. M. Jiménez, E. Bayo, and J. G. de Jalón, "A simple and highly parallelizable method for real-time dynamic simulation based on velocity transformation," *Comput. Methods Appl. Mech. Eng.*, vol. 107, no. 3, pp. 313–339, 1993.

[5] J. Watton, *Fluid Power Systems: Modeling, Simulation, Analog and Microcomputer Control*. Cambridge, U.K.: Prentice-Hall, 1989.

[6] S. Jaiswal, M. I. Islam, L. Hannola, J. Sopanen, and A. Mikkola, "Gamification procedure based on real-time multibody simulation," *Int. Rev. Model. Simul.*, vol. 11, no. 5, pp. 259–266, 2018.

[7] J. Rahikainen, A. Mikkola, J. Sopanen, and J. Gerstmayr, "Combined semi-recursive formulation and lumped fluid method for monolithic simulation of multibody and hydraulic dynamics," *Multibody Syst. Dyn.*, vol. 44, no. 3, pp. 293–311, 2018.

[8] J. Cuadrado, D. Dopico, M. Gonzalez, and M. A. Naya, "A combined penalty and recursive real-time formulation for multibody dynamics," *J. Mech. Des.*, vol. 126, no. 4, pp. 602–608, 2004.

[9] J. T. Cook, L. Ray, and J. Lever, "Multi-body dynamics model of a tracked vehicle using a towing winch for optimal mobility control and terrain identification," in *Proc. ASME Dyn. Syst. Control Conf.*, Minneapolis, MN, USA, 2016, pp. 1–8.

[10] Z. Zou, X. Pang, and J. Chen, "Comprehensive theoretical digging performance analysis for hydraulic excavator using convex polytope method," *Multibody Syst. Dyn.*, vol. 47, no. 2, pp. 137–164, 2019.

[11] A. Nicolini, F. Mocera, and A. Somà, "Multibody simulation of a tracked vehicle with deformable ground contact model," *Proc. Inst. Mech. Eng. K, J. Multi-Body Dyn.*, vol. 233, no. 1, pp. 152–162, 2018.

[12] M. G. Bekker, *Introduction to Terrain-Vehicle Systems*. Ann Arbor, MI, USA: Univ. of Michigan Press, 1969.

[13] Z. Janosi and B. Hanamoto, "The analytical determination of drawbar pull as a function of slip for tracked vehicles in deformable soils," in *Proc. 1st Int. Conf. Int. Soc. Terrain-Vehicle Syst.*, Turin, Italy, 1961, pp. 707–736.

[14] Z.-D. Ma and N. C. Perkins, "A super-element of track-wheel-terrain interaction for dynamic simulation of tracked vehicles," *Multibody Syst. Dyn.*, vol. 15, no. 4, pp. 347–368, 2006.

[15] A. Sandu, C. Sandu, and M. Ahmadian, "Modeling multibody systems with uncertainties. Part I: Theoretical and computational aspects," *Multibody Syst. Dyn.*, vol. 15, no. 4, pp. 369–391, 2006.

[16] C. Sandu, A. Sandu, and M. Ahmadian, "Modeling multibody systems with uncertainties. Part II: Numerical applications," *Multibody Syst. Dyn.*, vol. 15, no. 3, pp. 241–262, 2006.

[17] D. Holz, T. Beer, and T. Kuhle, "Soil deformation models for real-time simulation: A hybrid approach," in *Proc. 6th Workshop Virtual Reality Interact. Phys. Simulations*, Karlsruhe, Germany, 2009, pp. 21–30.

[18] D. Dopico, A. Luaces, and M. González, "A soil model for a hydraulic simulator excavator based on real-time multibody dynamics," in *Proc. 5th Asian Conf. Multibody Dyn.*, Kyoto, Japan, 2010, pp. 325–333.

[19] J. Cuadrado, J. Cardenal, and E. Bayo, "Modeling and solution methods for efficient real-time simulation of multibody dynamics," *Multibody Syst. Dyn.*, vol. 1, no. 3, pp. 259–280, 1997.

[20] K. Hunt and F. Crossley, "Coefficient of restitution interpreted as damping in vibroimpact," *J. Appl. Mech.*, vol. 42, no. 2, pp. 440–445, Jun. 1975.

[21] D. Dopico, A. Luaces, M. Gonzalez, and J. Cuadrado, "Dealing with multiple contacts in a human-in-the-loop application," *Multibody Syst. Dyn.*, vol. 25, no. 2, pp. 167–183, 2011.

[22] R. He, C. Sandu, A. K. Khan, A. G. Guthrie, P. S. Els, and H. A. Hamersma, "Review of terramechanics models and their applicability to real-time applications," *J. Terramech.*, vol. 81, pp. 3–22, Feb. 2019.

[23] J. Madsen, D. Negrut, A. Reid, A. Seidl, P. Ayers, G. Bozdech, J. Freeman, and J. O'Kins, "A physics based vehicle terrain interaction model for soft soil off-road vehicle simulations," *SAE Int. J. Commercial Vehicles*, vol. 5, no. 1, pp. 280–290, 2012.

[24] A. Jain, J. Balaram, J. Cameron, J. Guineau, C. Lim, M. Pomerantz, and G. Sohl, "Recent developments in the ROAMS planetary rover simulation environment," in *Proc. IEEE Aerosp. Conf.*, Big Sky, MT, USA, Mar. 2004, pp. 861–876.

[25] J. F. Labuz and A. Zang, "Mohr–Coulomb failure criterion," *Rock Mech. Rock Eng.*, vol. 45, no. 6, pp. 975–979, 2012.

[26] A. Azimi, J. Kövecses, and J. Angeles, "Wheel–soil interaction model for rover simulation and analysis using elastoplasticity theory," *IEEE Trans. Robot.*, vol. 29, no. 5, pp. 1271–1288, Oct. 2013.

[27] J.-Y. Wong and A. R. Reece, "Prediction of rigid wheel performance based on the analysis of soil-wheel stresses part I. Performance of driven rigid wheels," *J. Terramech.*, vol. 4, no. 1, pp. 81–98, 1967.

[28] E. Bayo, J. G. De Jalon, and M. A. Serna, "A modified Lagrangian formulation for the dynamic analysis of constrained mechanical systems," *Comput. Methods Appl. Mech. Eng.*, vol. 71, no. 2, pp. 183–195, 1988.

[29] E. Bayo and M. A. Serna, "Penalty formulations for the dynamic analysis of elastic mechanisms," *J. Mech., Transmiss., Autom. Des.*, vol. 111, no. 3, pp. 321–327, 1989.

[30] D. S. Bae, J. M. Han, and H. H. Yoo, "A generalized recursive formulation for constrained mechanical system dynamics," *Mech. Struct. Mach.*, vol. 27, no. 3, pp. 293–315, 1999.

[31] J. de García Jalón, E. Álvarez, F. A. de Ribera, I. Rodríguez, and F. J. Funes, "A fast and simple semi-recursive formulation for multi-rigid-body systems," *Advances in Computational Multibody Systems*, vol. 2. Dordrecht, The Netherlands: Springer, 2005, pp. 1–23.

[32] S. Gottschalk, M. C. Lin, and D. Manocha, "OBBTree: A hierarchical structure for rapid interference detection," in *Proc. 23rd Annu. Conf. Comput. Graph. Interact. Techn.*, New Orleans, LA, USA, 1996, pp. 171–180.

[33] E. Drumwright, "A fast and stable penalty method for rigid body simulation," *IEEE Trans. Vis. Comput. Graphics*, vol. 14, no. 1, pp. 231–240, Jan./Feb. 2008.

[34] C. C. de Wit, R. Horowitz, and P. Tsiotras, *New Directions in Nonlinear Observer Design*. London, U.K.: Springer, 1999.

[35] C. C. de Wit and P. Tsiotras, "Dynamic tire friction models for vehicle traction control," in *Proc. 38th IEEE Conf. Decis. Control*, Phoenix, AZ, USA, Dec. 1999, pp. 3746–3751.

[36] J. G. de Jalon and E. Bayo, *Kinematic and Dynamic Simulation of Multibody Systems: The Real-Time Challenge*. New York, NY, USA: Springer-Verlag, 1994.

[37] M. Pla-Castells, I. García-Fernández, and R. J. Martínez, "Approximation of continuous media models for granular systems using cellular automata," in *Proc. 6th Int. Conf. Cellular Automata Res. Ind.*, Amsterdam, The Netherlands, 2004, pp. 230–237.

[38] M. Pla-Castells, I. García-Fernández, and R. J. Martínez, "Interactive terrain simulation and force distribution models in sand piles," in *Proc. 7th Int. Conf. Cellular Automata Res. Ind.*, Perpignan, France, 2006, pp. 392–401.

[39] J.-P. Bouchaud, M. E. Cates, J. R. Prakash, and S. F. Edwards, "A model for the dynamics of sandpile surfaces," *J. Phys. I, France*, vol. 4, no. 10, pp. 1383–1410, 1994.

[40] H. M. Handroos and M. J. Vilenius, "Flexible semi-empirical models for hydraulic flow control valves," *J. Mech. Des.*, vol. 113, no. 3, pp. 232–238, 1991.

[41] M. Moore and J. Wilhelms, "Collision detection and response for computer animation," in *Proc. 15th Annu. Conf. Comput. Graph. Interact. Techn.*, Atlanta, GA, USA, 1988, pp. 289–298.

**SURAJ JAISWAL** was born in Kolkata, India, in July 29, 1991. He received the B.E. degree in production engineering from Jadavpur University, Kolkata, in 2013, and the M.S. degree in mechanical engineering from the Lappeenranta University of Technology, Lappeenranta, Finland, in 2017, where he is currently pursuing the Ph.D. degree in mechanical engineering.

From 2013 to 2015, he worked as a Design Engineer at Tata Consultancy Services Ltd., Kolkata. Since 2016, he has been working as a Junior Research Assistant at the Lappeenranta University of Technology. His research interests include multibody system dynamics, real-time simulation, and vehicle dynamics.

Mr. Jaiswal received the "On the Spot Award" for an outstanding contribution to Tata Consultancy Services Ltd., in 2013, and the "Best Paper Award" at the 9th Asian Conference on Multibody Dynamics (ACMD 2018), Xi'an, China, in August 2018.

**PASI KORKEALAAKSO** was born in Finland, in 1977. He received the M.S. degree in mechanical engineering and the Ph.D. degree from the Lappeenranta University of Technology, Lappeenranta, Finland, in 2002 and 2009, respectively.

From 2002 to 2010, he had been a part of several research projects financed by the Academy of Finland and the National Technology Agency of Finland (TEKES). He is currently the Co-Owner and the Technical Director at Mevea Ltd., Finland. His research interests cover topics related to multibody modeling methods, the modeling and control of hydraulically driven systems, machine–environment interaction models, and real-time simulation software development.

**RAFAEL ÅMAN** was born in Karkkila, Finland, in 1978. He received the B.S. degree in mechanical engineering (mechatronics) from the Helsinki University of Applied Sciences (Stadia), Finland, in 2002, and the M.S. and Ph.D. degrees in mechanical engineering (mechatronics) from the Lappeenranta University of Technology, Lappeenranta, Finland, in 2007 and 2011, respectively.

From 2006 to 2016, he worked as a Researcher on the simulation of fluid power circuits, hybrid power transmission, and energy recovery systems at the Lappeenranta University of Technology. He has work experience as a Service Engineer in a civil engineering company. Since 2016, he has been with AGCO Corporation. He works at Valtra Inc., Suolahti, Finland. His main responsibilities have included system simulations and tractor design validation tests, as well as research and advanced engineering. As a Technical Specialist, he focuses on the use of future technologies in agricultural machinery and in their Research and Development processes. He has contributed to 26 scientific publications and presentations.

**JUSSI SOPANEN** (M'14) was born in Enonkoski, Finland, in 1974. He received the M.S. degree in mechanical engineering and the Ph.D. degree (in technology) from the Lappeenranta University of Technology, Lappeenranta, Finland, in 1999 and 2004, respectively.

From 1999 to 2006, he worked as a Researcher at the Department of Mechanical Engineering, Lappeenranta University of Technology. From 2004 to 2005, he worked as a Product Development Engineer at Rotatek Finland Ltd., electric machine manufacturer. From 2006 to 2012, he worked as a Principal Lecturer of mechanical engineering and the Research Manager at the Faculty of Technology, Saimaa University of Applied Sciences, Lappeenranta. He is currently a Professor in machine dynamics with the Lappeenranta University of Technology. His research interests are in rotor dynamics, multibody dynamics, and the mechanical design of electrical machines.

**AKI MIKKOLA** received the Ph.D. degree in machine design, in 1997.

Since 2002, he has been working as a Professor at the Department of Mechanical Engineering, Lappeenranta University of Technology, Lappeenranta, Finland. He is currently leading the research team of the Laboratory of Machine Design, Lappeenranta University of Technology. His research interests include machine dynamics and vibration, multibody system dynamics, and bio-mechanics. He has been awarded five patents and has contributed to more than 90 peer-reviewed journal articles.